

# Deep learning as a tool to distinguish between high orbital angular momentum optical modes

E. M. Knutson<sup>a</sup>, Sanjaya Lohani<sup>a</sup>, Onur Danacı<sup>a</sup>, Sean D. Huver<sup>b</sup>, and Ryan T. Glasser<sup>a</sup>

<sup>a</sup>Tulane University, 6823 St. Charles Ave, New Orleans, LA, USA

<sup>b</sup>Deep Science AI, 10 Taylor Pl, Eatontown, NJ, USA

## ABSTRACT

The generation of light containing large degrees of orbital angular momentum (OAM) has recently been demonstrated in both the classical and quantum regimes. Since there is no fundamental limit to how many quanta of OAM a single photon can carry, optical states with an arbitrarily high difference in this quantum number may, in principle, be entangled. This opens the door to investigations into high-dimensional entanglement shared between states in superpositions of nonzero OAM. Additionally, making use of non-zero OAM states can allow for a dramatic increase in the amount of information carried by a single photon, thus increasing the information capacity of a communication channel. In practice, however, it is difficult to differentiate between states with high OAM numbers with high precision. Here we investigate the ability of deep neural networks to differentiate between states that contain large values of OAM. We show that such networks may be used to differentiate between nearby OAM states that contain realistic amounts of noise, with OAM values of up to 100. Additionally, we examine how the classification accuracy scales with the signal-to-noise ratio of images that are used to train the network, as well as those being tested. Finally, we demonstrate the simultaneous classification of  $> 100$  OAM states with greater than 70% accuracy. We intend to verify our system with experimentally-produced classical OAM states, as well as investigate possibilities that would allow this technique to work in the few-photon quantum regime.

**Keywords:** Orbital angular momentum, machine learning, deep learning, neural networks

## 1. INTRODUCTION

A fundamental goal in optical communications is to maximize the amount of information that one may store in and transmit with light. Current optical fiber systems are reaching limits imposed by nonlinear effects,<sup>1</sup> but spatial-division-multiplexing methods offer a potential solution to bypass such limitations. One promising route toward achieving this is by making use of the orbital angular momentum (OAM) degree-of-freedom of light, which in principle has infinite degrees of freedom, allowing for potential orders-of-magnitude increases in information transfer rates<sup>2,3</sup>. Classical fields of light containing OAM, such as Laguerre-Gauss (LG) and Bessel-Gauss (BG) modes, have been used to successfully demonstrate bit transmission rates of  $> 1$  Terabit per second in both free-space and fiber systems.<sup>4,5</sup> However, these results have been constrained by the maximum number of simultaneously detectable OAM modes, which is currently 16.<sup>6</sup> Additionally, polarization entanglement in Gaussian modes has been successfully transferred to the OAM degree-of-freedom ( $l$ ) of photons up to  $l = \pm 300$ .<sup>7</sup> However, the detection method used suffers from adding unwanted loss to the optical state, and requires increasingly precise alignment and resolution as the degree of OAM is increased. Another commonly used method of OAM detection relies on the use of cascaded Mach-Zehnder interferometers, which is not an easily scalable approach. Furthermore, these methods require bulky optical devices, making their integration into a compact platform troublesome. Alternatives have recently appeared in the form of plasmonic lenses,<sup>8</sup> as well as a simple shallow neural network for visual classification of OAM intensity profiles.<sup>6</sup> The plasmonics lens solution requires the use of a near-field scanning optical microscope as well as additional numerical techniques to classify OAM

---

Further author information:

R.T.G.: E-mail: rglasser@tulane.edu

E.M.K.: E-mail: eknutson@gmail.com

S.D.H.: E-mail: huvers@deepscience.ai

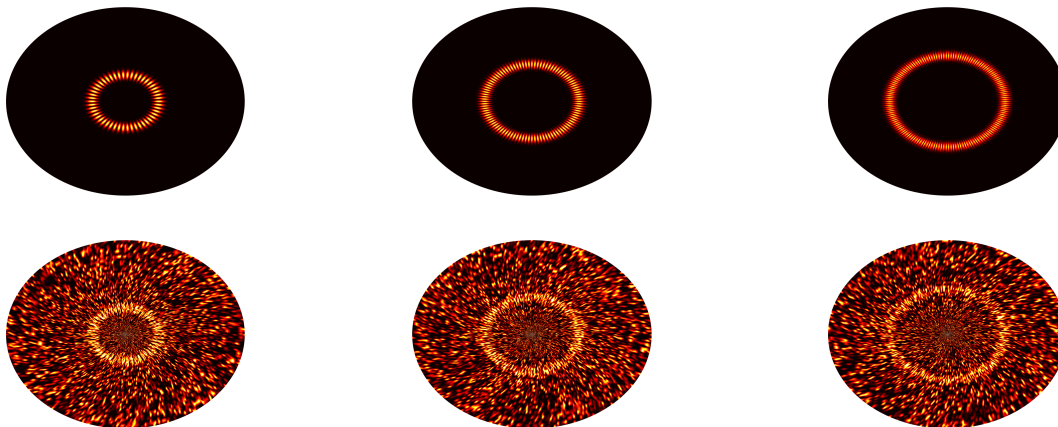
modes. The near-field scanning microscope is a major impediment to any compact integration effort, much like cascaded interferometers. The shallow (i.e. no more than one hidden layer between input and output, as described below) neural network, so far the most successful method of simultaneous discrimination, is capable of discriminating 16 different types of OAM superposition modes simultaneously after free-space transmission through turbulent city atmosphere. We expand on this concept by making use of more state-of-the-art machine learning techniques that involve deep neural networks, which have proven quite successful in image classification scenarios. Here we present a deep neural network capable of correctly identifying the OAM (superposition) state of numerically-produced noisy test images, as well as a network capable of simultaneously differentiating 110 OAM superposition states with an accuracy of  $> 70\%$ , bypassing the need for un-scalable bulky resources altogether, while allowing for a substantial increase in the number of simultaneously-discriminated OAM modes. These results have potential revolutionary benefits to increasing communication information rates, not only for classical communications, but for quantum applications as well, such as quantum key distribution.<sup>9</sup>

## 2. OPTICAL MODES WITH NON-ZERO OAM

In cylindrical coordinates, the natural solutions of the paraxial wave equation are Laguerre-Gauss modes. These modes have a spiral phase distribution  $e^{il\phi}$ , creating a phase singularity and therefore a region of zero intensity along the beam axis. The phase advances smoothly with angle; for  $l = \pm 1$ , points at opposite sides of the vortex are  $180^\circ$  out of phase. Light possessing a single topological charge forms the shape of a ring, with inner radius directly proportional to  $|l|$ . Perhaps more applicable to quantum information experiments, light in superpositions of OAM modes develop unique interference patterns with  $2l$  maxima arranged along this ring, making them prime candidates for machine learning training images. The state of these superposition modes may be written as

$$|\text{LG}_{\pm l}^\alpha\rangle = \frac{1}{\sqrt{2}} (|\text{LG}_{+l}\rangle + e^{i\alpha}|\text{LG}_{-l}\rangle) \quad (1)$$

where  $\alpha$  denotes the relative phase between the two modes, which corresponds to a rotation of the phase and intensity structure. These states can theoretically carry OAM of arbitrarily high integer ( $l$ ) value.



(a) superposition of  $l=\pm 25$

(b) superposition of  $l=\pm 50$

(c) superposition of  $l=\pm 75$

Figure 1: Computer-generated training images for the machine learning software, in superpositions of different OAM values. Random noise was added to the images in the bottom row to approximate laboratory conditions. The average signal-to-noise ratios for each are (a) 0.602, (b) 0.690 and (c) 0.704. The images are generated using a modified version of the “basic paraxial optics toolkit” with Matlab.<sup>10</sup>

Several different methods exist to generate LG modes of increasing orders. The most straightforward method is the use of diffraction gratings. A standard diffraction grating consisting of parallel lines leads to diffracted orders in  $l = 0$  states. To achieve, for example, an  $l = 1$  state, the Gaussian beam needs to travel through

a central “fork” dislocation diffraction grating that contains exactly one more line above the dislocation than below. The first-order diffracted output modes then contain  $l = \pm 1$  quanta of OAM. Higher OAM states can be created by increasing the difference in the number of lines above and below the dislocation, or interfering higher-order Laguerre-Gauss modes.<sup>11</sup> Then, interfering the  $+l$  and  $-l$  modes results in the desired superposition states. Experimentally, however, these masks have finite resolution and result in imperfect OAM modes, making it difficult to produce pure OAM states when approaching large values of  $l$ . Newer methods that make use of spatial-light modulators have allowed for a significant increase in the degree of OAM that may be imparted on an optical mode, allowing for the generation of the aforementioned entangled  $l = \pm 300$  state.<sup>7</sup>

While having received much attention, LG beams are not the only optical states that contain nonzero OAM. In particular, Bessel-Gauss beams, above the zeroth order, contain increasingly large degrees of OAM, in an similar manner to LG modes. In addition, BG beams have been shown to exhibit novel properties such as “self-healing” after encountering an obstacle as well as limited diffraction upon propagation as compared to a typical Gaussian mode.<sup>12-15</sup> The combination of nonzero OAM, limited-diffraction, and self-healing makes BG modes an interesting prospect for robust, high-information transfer rate optical communication. While it is also possible to produce higher-order Bessel-Gauss beams with spatial light modulators, recent work has shown promising methods of generating nearly BG modes via nonlinear processes involving light-atom interactions.<sup>16</sup> As these BG modes are of increasing interest to optical communication and imaging schemes, we plan to extend our present results to test the effectiveness of deep neural networks on classifying such modes that have undergone realistic propagation, and have experienced loss and mode distortion after encountering obstacles.

Here, we generate computer-simulated superpositions of Laguerre-Gauss modes from  $l = 1$  to  $l = 110$  to be used as training images for our deep neural networks. These images have varying amounts of Gaussian white noise and multiplicative noise added to them, in order to simulate non-ideal experimental conditions. This also allows for the investigation of how the neural networks perform as the signal-to-noise ratio of the training, and (or) test images, is varied. Typical images are shown above in the bottom row of Figure 1.

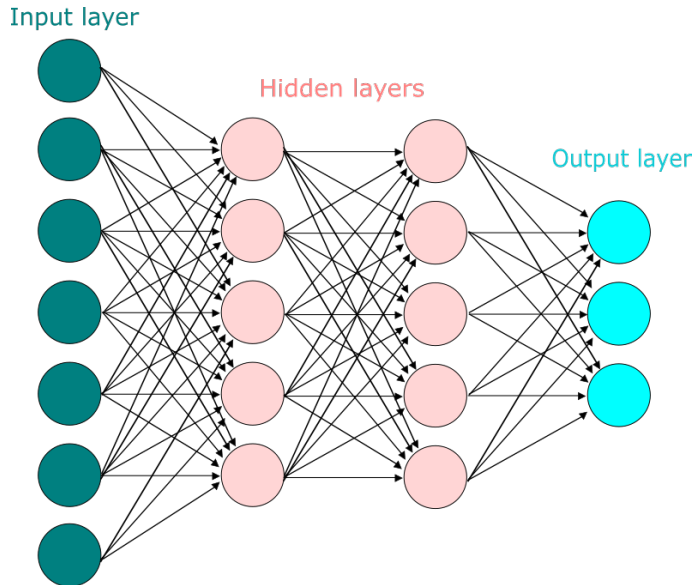


Figure 2: Schematic of a deep neural network that has two hidden layers. The input layer is connected to a specified number of neurons in the first hidden layer. This continues until the output layer is reached, whose output corresponds to the resulting classification of the input (image). As an example, the deep neural network used here to individually classify OAM states contains 18150 input neurons, and 3 hidden layers that each contain 20 neurons. The output layer consists of either 100 or 110 neurons, depending on what values of OAM the training images contain (from  $l = 1$  up to either  $l = 100$  or  $110$ ).

### 3. DEEP LEARNING

Artificial neural networks, like other machine learning methods, are used to solve tasks that are difficult to solve using standard rule-based programming (for example, handwriting recognition). The general form of a neural network contains an input layer and an output layer composed of artificial neurons, with “hidden” layers in between, as shown schematically in Figure 2. In general, each neuron applies a nonlinear transformation on its weighted and biased input, then applies an activation function before the feed-forward process to the next layer of neurons. A learning algorithm is then used to back-propagate error, which results in the network’s ability to learn. A neural network whose number of hidden layers is greater than 1 is referred to as a deep neural network (DNN), and their study is broadly referred to as “deep learning.” Deep neural networks inherently allow for significantly increased tiers of abstraction due to the presence of multiple hidden layers, which allows for the recognition and classification of increasingly complex patterns and decision making.

The field of deep learning has seen explosive growth since 2012, when a seven-layer DNN won the annual ImageNet computer vision classification competition.<sup>17</sup> DNNs until this point had been mostly dismissed as too computationally expensive and without much practical promise. However, this pessimism began to change with the confluence of several factors. First, graphical processing units (GPUs) were shown to offer massive parallel speedups in neural network calculations, allowing models of increasing complexity to be built relatively cheaply in terms of computational resources. Second, biologically-inspired hierarchical models, such as convolutional neural networks (CNNs), showed better performance than previous deep models where all neurons in successive layers were simply connected to each other.<sup>18</sup> These new sparser models were not only faster to train, but also proved to be more accurate.

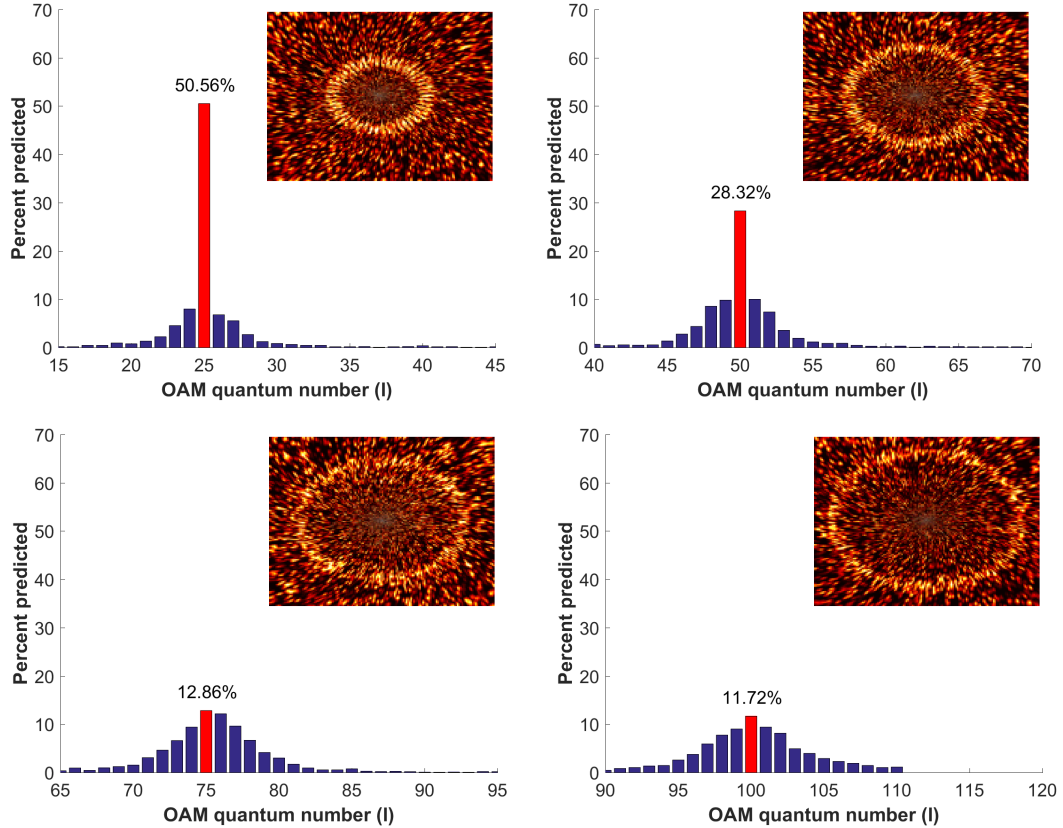


Figure 3: Prediction accuracy percentages for test images in superpositions of various  $l$  values (top left: 25, top right: 50, bottom left: 75, bottom right: 100) using the Cypress supercomputer. The correct  $l$  value is highlighted in red. The average signal-to-noise ratio of these test images (shown to the right of each plot) was 0.599.

## 4. RESULTS

Here we make use of two separate DNNs, one which we utilize for the individual classification of OAM states with varying signal-to-noise ratios, and one of which performs the simultaneous classification of  $> 100$  OAM modes with high accuracy. The former is run on Tulane University’s “Cypress” supercomputer, composed of an Intel Ivy Bridge CPU, Intel Xeon Phi co-processor, and Lustre file system running on Dell storage with Intel Enterprise Edition for Lustre (IEEL) technology.<sup>19</sup> This DNN uses a stochastic gradient descent algorithm, which continuously updates the weights and biases of each neuron before coming to an output prediction. Each prediction ends an “epoch,” and a new epoch is started with the optimized weights and biases of the last. A single trial corresponds to the classification of the test image after 50 epochs. Additionally, this DNN uses supervised learning, i.e. the network is given the correct  $l$  of each training image. As is standard in machine learning algorithms, we must find the optimal performance settings of the network, known as hyperparameters. The optimal learning rate  $\eta$ ,<sup>20</sup> for example, is chosen manually for each training set, and is often a trade-off between high accuracy and short computation time.

The DNN for individual classification described above contains 18150 input layer neurons (equal to the number of pixels in the training/test images), three hidden layers with 20 neurons in each hidden layer, and either 100 or 110 output layer neurons (depending on if the classification is extended to  $l = 100$  or 110). A single training set consists of 20000 images that contain variable amounts of Gaussian and multiplicative (speckle) noise, examples of which are shown in the insets of Figure 3. The network successfully classifies OAM states up to  $l = 100$ , even with very noisy training and test images (down to a signal-to-noise ratio of  $\approx 0.27$ ), after 100 trials. The prediction accuracy after 100 trials with test images consisting of  $l = 25, 50, 75,$  and  $100$  is shown in Figure 3. The average signal-to-noise ratio of the test images is 0.599. The behavior of the network with increasing

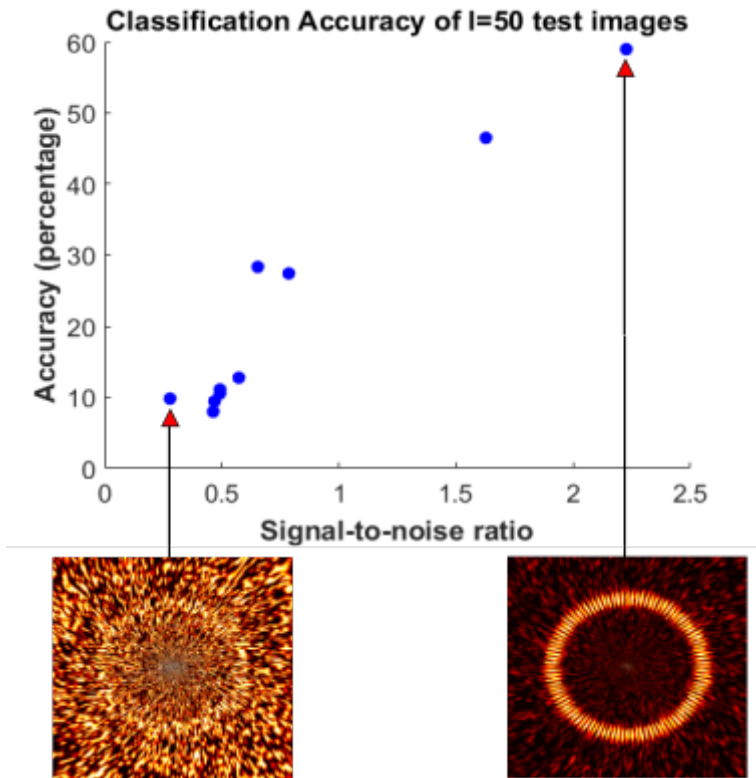


Figure 4: Classification accuracy of our deep neural network versus signal-to-noise ratio of the (training and test) images, after 100 trials with the same test image on the Cypress supercomputer. Each trial classifies the test image after 50 epochs. Note that regardless of accuracy percentage, the correct OAM value of  $l = 50$  was always the most frequently-predicted OAM value (as seen in Fig. 3).

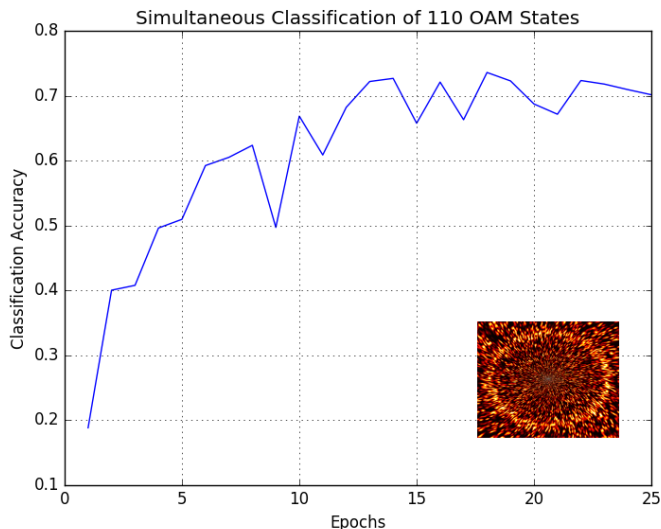


Figure 5: Classification accuracy for simultaneous discrimination of 110 OAM states with respect to training epochs on Deep Science AI’s Nvidia Titan X. A pre-trained version of the 16 layer network VGG16 was used. Further enhancements may come from increasing the number of training examples, as well as model parameter tuning. The images trained on and tested here have an average SNR of 0.517. An example image with  $l = 100$  is shown in the inset.

average signal-to-noise ratio of both training images and test images is shown in Figure 4. When the training images and the test image have a signal-to-noise ratio of  $\approx 2.3$ , the accuracy of this network in predicting the OAM value of an  $l = 50$  test image improves to nearly 60%.

In order to perform the simultaneous classification of a large number of OAM states of different orders, we used the 16 layer VGG16 network at Deep Science AI using an Nvidia Titan X GPU.<sup>21</sup> We began with a version of VGG16 that was pre-trained on the ImageNet dataset<sup>17</sup> as studies have shown that pre-trained networks learn new classifications faster than those that are untrained, while also requiring less training data.<sup>22</sup> Using this model, we have achieved an accuracy of  $> 74\%$  in the simultaneous classification of 110 different OAM states. Figure 5 shows the accuracy of this simultaneous classification as the number of epochs is increased. We anticipate that even higher accuracies will be reached as we increase the resolution of the training and test images used.

## 5. CONCLUSIONS

In this manuscript we have demonstrated the ability of deep neural networks to effectively classify states that contain large degrees of orbital angular momentum. We show that such deep learning techniques are able to successfully perform orbital angular momentum classification even in a low signal-to-noise ratio regime, for OAM values of up to  $l = 100$ . Additionally, we have shown that a 16 layer deep neural network can perform the simultaneous classification of 110 different orbital angular momentum superposition states with greater than 74% accuracy. We anticipate that these results may stimulate the use of deep learning techniques applied to both classical and quantum optics experiments, as well as a variety of communication protocols.

## ACKNOWLEDGMENTS

RTG would like to acknowledge support from Northrop Grumman - *NG NEXT*, as well as the Louisiana State Board of Regents.

## REFERENCES

- [1] Richardson, D. J., “Filling the light pipe,” *Science* **330**(6002), 327–328 (2010).
- [2] Torres, J. and Torner, L., [*Twisted Photons: Applications of Light with Orbital Angular Momentum*], Bristol: Wiley-VCH (2011).
- [3] Andrews, D. and Babiker, M., [*The Angular Momentum of Light*], Cambridge: Cambridge University Press (2012).
- [4] Wang, J., Yang, J.-Y., Fazal, I. M., Ahmed, N., Yan, Y., Huang, H., Ren, Y., Yue, Y., Dolinar, S., Tur, M., and Willner, A. E., “Terabit free-space data transmission employing orbital angular momentum multiplexing,” *Nature Photonics* (2007).
- [5] Bozinovic, N., Yue, Y., Ren, Y., Tur, M., Kristensen, P., Huang, H., Willner, A. E., and Ramachandran, S., “Terabit-scale orbital angular momentum mode division multiplexing in fibers,” *Science* **340**(6140), 1545–1548 (2013).
- [6] Krenn, M., Fickler, R., Fink, M., Handsteiner, J., Malik, M., Scheidl, T., Ursin, R., and Zeilinger, A., “Communication with spatially modulated light through turbulent air across Vienna,” *New Journal of Physics* **16**(11), 113028 (2014).
- [7] Fickler, R., Lapkiewicz, R., Plick, W. N., Krenn, M., Schaeff, C., Ramelow, S., and Zeilinger, A., “Quantum entanglement of high angular momenta,” *Science* **338**(6107), 640–643 (2012).
- [8] Liu, A. P., Xiong, X., Ren, X. F., Cai, Y. J., Rui, G. H., Zhan, Q. W., Guo, G. C., and Guo, G. P., “Detecting orbital angular momentum through division-of-amplitude interference with a circular plasmonic lens,” *Nature Scientific Reports* **3** (2013).
- [9] Mirhosseini, M., Magaña-Loaiza, O., O’Sullivan, M. N., Rodenburg, B., Malik, M., Gauthier, D. J., and Boyd, R. W., “High-dimensional quantum cryptography with twisted light,” **17**, 033033 (2014). <http://arxiv.org/abs/1402.7113>.
- [10] Gretarsson, A. M., “Basic paraxial optics toolkit.” <https://www.mathworks.com/matlabcentral/fileexchange/15459-basic-paraxial-optics-toolkit>.
- [11] Padgett, M., Arlt, J., Simpson, N., and Allen, L., “An experiment to observe the intensity and phase structure of laguerregaussian laser modes,” *American Journal of Physics* **64**(1), 77–82 (1996).
- [12] Durnin, J., Miceli, J. J., and Eberly, J. H., “Diffraction-free beams,” *Physical Review Letters* **58**, 1499–1501 (Apr. 1987).
- [13] Gori, F., Guattari, G., and Padovani, C., “Bessel-Gauss beams,” *Optics Communications* **64**, 491–495 (Dec. 1987).
- [14] McGloin, D. and Dholakia, K., “Bessel beams: diffraction in a new light,” *Contemporary Physics* **46**, 15–28 (Jan. 2005).
- [15] Herman, R. M. and Wiggins, T. A., “Production and uses of diffractionless beams,” *Journal of the Optical Society of America A* **8**, 932–942 (June 1991).
- [16] Danaci, O., Rios, C., and Glasser, R. T., “All-optical mode conversion via spatially multimode four-wave mixing,” *New Journal of Physics* **18**(7), 073032 (2016).
- [17] Krizhevsky, A., Sutskever, I., and Hinton, G. E., “Imagenet classification with deep convolutional neural networks,” in [*Advances in Neural Information Processing Systems*], 2012.
- [18] Matsugu, M., Mori, K., Mitari, Y., and Kaneda, Y., “Subject independent facial expression recognition with robust face detection using a convolutional neural network,” *Neural Networks* **16**(56), 555 – 559 (2003). *Advances in Neural Networks Research: {IJCNN} ’03*.
- [19] “Cypress: High performance computing system.” <https://crsc.tulane.edu/>. Accessed: 2016-07-20.
- [20] Nielsen, M., [*Neural Networks and Deep Learning*], Determination Press (2015).
- [21] Deng, J., Dong, W., Socher, R., jia Li, L., Li, K., and Fei-fei, L., “Imagenet: A large-scale hierarchical image database,” in [*In CVPR*], (2009).
- [22] Larochelle, H., Bengio, Y., Louradour, J., and Lamblin, P., “Exploring strategies for training deep neural networks,” *J. Mach. Learn. Res.* **10**, 1–40 (June 2009).